Subsurface melting of a free-floating Antarctic iceberg

Gordon R. Stephenson Jr.[a,*], Janet Sprintall[a], Sarah T. Gille[a], Maria Vernet[a], John J. Helly[b], Ronald S. Kaufmann[c]

[a] Scripps Institution of Oceanography, University of California–San Diego, 9500 Gilman Dr. Mail Code 0230, La Jolla, CA 92093, USA
[b] San Diego Supercomputer Center, University of California–San Diego, 9500 Gilman Dr. Mail Code 0505, La Jolla CA 92093, USA
[c] Marine Science and Environmental Studies Department, University of San Diego, 5998 Alcalá Park, San Diego, CA 92110, USA

ARTICLE INFO

ABSTRACT

Observations near a large tabular iceberg in the Weddell Sea in March and April 2009 show evidence that water from ice melting below the surface is dispersed in two distinct ways. Warm, salty anomalies in $T–S$ diagrams suggest that water from the permanent thermocline is transported vertically as a result of turbulent entrainment of meltwater at the iceberg's base. Stepped profiles of temperature, salinity, and density in the seasonal thermocline are more characteristic of double-diffusive processes that transfer meltwater horizontally away from the vertical ice face. These processes contribute comparable amounts of meltwater–$O(0.1 \ m^3)$ to the upper 200 m of a 1 m^2 water column–but only basal melting results in significant upwelling of water from below the Winter Water layer into the seasonal thermocline, suggesting that these two processes may have different effects on vertical nutrient transport near an iceberg.

1. Introduction

Calving from glaciers in Antarctica accounts for 2000 Gt of yearly freshwater input into the Southern Ocean, half of which takes the form of large tabular icebergs (Jacobs et al., 1992). Icebergs with a major axis larger than 10 nautical miles are responsible for most of the transport of freshwater north of 63°S (Silva et al., 2006). Drifting icebergs redistribute heat and freshwater, and transport trace metals (Smith et al., 2007). Their effects on surface temperature and salinity alter local stratification and may affect the rates of sea-ice formation and Antarctic Bottom Water formation (Jongma et al., 2009). Because icebergs tend to follow well-defined tracks determined by prevailing winds and currents, they have enhanced impacts on specific regions (Jenkins, 1999). For example, in regions with high iceberg concentrations, such as the Weddell Sea, iceberg meltwater can contribute as much to the freshwater balance as precipitation minus evaporation (Silva et al., 2006).

Recent studies have shown that the wake of an iceberg is associated with an increase in surface chlorophyll concentration (Schwarz et al., 2009). Melting ice contains biologically important micronutrients such as iron (Lin et al., 2011) and may be enriched in nitrate and nitrite (Vernet et al., 2011). Concentrations of other nutrients, such as phosphate and silicate, generally increase with depth in the Weddell Sea (Vernet et al., 2011; Neshyba, 1977). Icebergs can, therefore, increase nutrient supply near the surface directly in their meltwater (Smith et al., 2007), or by melting at their base that entrains deep water and causes it to upwell (Neshyba, 1977). There has been considerable debate, however, concerning the location where most melting occurs, the vertical displacement of meltwater, and the amount of ambient water entrained by upwelling meltwater.

Donaldson (1978) summarized three possibilities for meltwater distribution from ice melting below the ocean surface. First, if little entrainment of surrounding water occurs, meltwater will rise in a relatively thin layer and spread horizontally at the surface as a lens of freshwater. Cooling and freshening of surface water near an iceberg are discussed by Helly et al. (2011). Second meltwater that entrains a large amount of ambient water from below the permanent thermocline can rise and appear as a $T–S$ anomaly higher in the water column. Such anomalies have been observed near Pine Island Glacier (Jenkins, 1999). Third meltwater can spread horizontally in stratified layers, resulting in steps in hydrographic profiles. These steps are a common feature of profiles in the Weddell Sea (Huppert and Turner, 1980, hereafter HT80) and have also been measured near the edge of the Erebus Glacier Tongue (Jacobs et al., 1981) and near an iceberg frozen into fast ice (Ohshima et al., 1994).

Here, we present evidence for upwelled meltwater mixtures and horizontal motion of meltwater in stratified layers observed near a free-floating iceberg in the Weddell Sea. These two types of melting are identified in $T–S$ diagrams and potential density

* Corresponding author.
  E-mail addresses: grstephe@ucsd.edu (G.R. Stephenson Jr.), jsprintall@ucsd.edu (J. Sprintall), sgille@ucsd.edu (S.T. Gille), mvernet@ucsd.edu (M. Vernet), hellyj@ucsd.edu (J.J. Helly), kaufmann@sandiego.edu (R.S. Kaufmann).

profiles and their freshwater contributions to the ocean near the iceberg are estimated.

2. Background

2.1. Turbulent mixing of meltwater

When ice melts in sea water, two opposing effects on density result. Heat transferred from ocean water to ice raises the ice temperature and effects a phase change, which requires L (344 kJ kg^{-1}) times the mass of ice to be melted, where L is the heat of fusion. As heat is used to melt ice, ambient water is cooled, which increases its density. At the same time, a reduction of salinity by dilution with fresh meltwater makes the ambient water less dense. For a range of temperatures and salinities including values typical of the Southern Ocean ($T < 10\,°C, S > 20$ psu), the reduction in salinity dominates, making meltwater mixtures positively buoyant (Gade, 1993). Assuming (1) equal effective diffusivities of heat and salt, as can occur in turbulent mixing, and (2) conservative mixing of meltwater and ambient water, melting of ice by sea water produces a mixture that can be described by a linear relation between temperature and salinity (Gade, 1979). Overcoming the heat of fusion requires 80 times the heat required to raise the temperature of the same mass of liquid water by 1 °C. The melting of ice by ocean water can, therefore, be treated as mixing of two water masses, one with the properties of the ambient water where melting occurs, and one with a salinity of 0 and an effective potential temperature of around $-80\,°C$ (or cooler, depending upon the internal temperature of the ice). The intersection of this meltwater mixing line with the freezing temperature at a given salinity and pressure dictates the maximum amount of melting that the ambient water can induce. This sets an upper limit on the concentration of meltwater attainable, assuming there is no external source of heat, of about 1% per °C elevation of ambient temperature above freezing (Jenkins, 1999).

In T–S space, this meltwater mixing line intercepts the temperature and salinity of ambient water at the depth at which melting occurs. This line has a characteristic slope

$$\left(\frac{\partial T}{\partial S}\right)_{melt} = \frac{\Delta T + Lc_p^{-1}}{S}, \tag{1}$$

where ΔT (°C) is the elevation of ambient temperature above the freezing point of water at salinity S (psu), $L = 334$ kJ kg^{-1} is the latent heat of fusion of water, and $c_p = 4.2$ J kg^{-1} °C^{-1} is the specific heat capacity of water (Gade, 1979).

Because the addition of meltwater to seawater makes the mixture less dense, the meltwater mixture rises to a level at which it is neutrally buoyant. The relative slopes of the T–S curve of the ambient water column, $(\partial T / \partial S)_{ambient}$, and the meltwater mixing line determines how upwelled meltwater mixtures appear. Where the T–S slope within a water column is steeper than $(\partial T / \partial S)_{melt}$, meltwater mixtures will appear as intrusions that are anomalously warm and salty relative to the water surrounding them at their new, neutrally buoyant level (Jenkins, 1999). Where $(\partial T / \partial S)_{ambient}$ is less than $(\partial T / \partial S)_{melt}$, upwelled meltwater mixtures will appear cooler and fresher relative to unaffected water at the same density.

2.2. Double-diffusive mixing of meltwater

In the absence of turbulent mixing, the assumption of equal effective diffusivities for heat and salt in Eq. (1) is no longer valid. The molecular diffusivity of heat is two orders of magnitude higher than that of salt, which can lead to double-diffusion. Under the right conditions, double-diffusion can result in the formation of thermohaline staircases (e.g. Morell et al., 2006). Near an ice face,

melting into a vertical salinity gradient can lead to these "stepped" profiles of temperature, salinity, and density with depth. Thermohaline staircases also occur in the open ocean as a result of salt-fingering, where warm, salty water overlies cool, fresh water, or diffusive convection, where cool, fresh water overlies warm, salty water (Schmitt, 1994).

In a series of laboratory experiments, HT80 melted vertical ice blocks in a tank of water stratified with a uniform vertical salinity gradient. Melting along a "sloped ceiling" of ice (Jacobs et al., 1981) or a vertical wall (HT80) in a salinity gradient leads to a series of vertically stacked circulation cells. These cells are visible as horizontal layers of uniform density separated by thin interfaces with a large density gradient. For experiments at a range of oceanic values of temperature and salinity, HT80 derived an empirical equation for layer thickness, h,

$$h = \frac{0.65[\rho(T_{fp},S) - \rho(T,S)]}{\frac{\partial \rho}{\partial z}}, \tag{2}$$

where density, ρ, is a function of the depressed freezing point near the ice, T_{fp}, the unperturbed salinity, S, and the unperturbed temperature, T.

Each circulation cell draws in ambient, unperturbed water near the top of the cell (Malki-Epshtein et al., 2004). This water cools near the ice face, is freshened slightly by entrainment of meltwater, and flows out near the bottom of the cell. As water flows out, it is warmed by thermal diffusion across the lower interface and rises slightly. Water flowing in along the top of a cell is cooled in a similar fashion, giving a tilt to the isopycnal layers. Most of the meltwater coming off the ice ends up vertically displaced to 2–3 layer thicknesses above where it formed (Malki-Epshtein et al., 2004).

In this paper, we use Eq. (1) to identify water in T–S diagrams and Eq. (2) to identify water in density profiles that has been influenced by two modes of melting (turbulent or double-diffusive, respectively). We then estimate where each type of melting occurs and gauge the amount of contributed meltwater and the direction (vertical or horizontal) of transport. Our ultimate goal is to understand the implications of iceberg meltwater for nutrient transport and biological productivity.

3. Data and methods

In March and April 2009, a cruise on the RV/IB Nathaniel B. Palmer (NBP) to the Powell Basin (Fig. 1) in the Weddell Sea east of the Antarctic Peninsula was undertaken to assess the impacts of icebergs on their biological, chemical, and physical environment. The main object of study was a large tabular iceberg designated C-18a. The iceberg C18 calved from the Ross Ice Shelf in 2002; C-18a is a fragment of C18 that has been tracked by satellite since 2005 (Stuart and Long, 2011). Helly et al. (2011) estimated the size of C-18a at about 35 km by 6 km with an average height above the water line of 28 m. During the cruise, Sherlock et al. (2011) used a remote operated vehicle (ROV) to examine the subsurface face of C-18a directly. The maximum depth of ice recorded by a sonar onboard the ROV was 190 m. Since melting is likely to be greater at the edge of the iceberg, where this measurement was taken, the base of C-18a may have been deeper closer to the center of the iceberg. C-18a travelled about 200 km from March 9 to April 1, following a clockwise path around the Powell Basin (Fig. 1B). The approximate position of C-18a was estimated from a combination of the ship's location while circumnavigating the iceberg, position fixes from the navigational radar of the NBP, and interpolation in time and space when no direct measurements were available.

This paper focuses on temperature and salinity profiles from 65 CTD casts taken over the course of the cruise. Results from
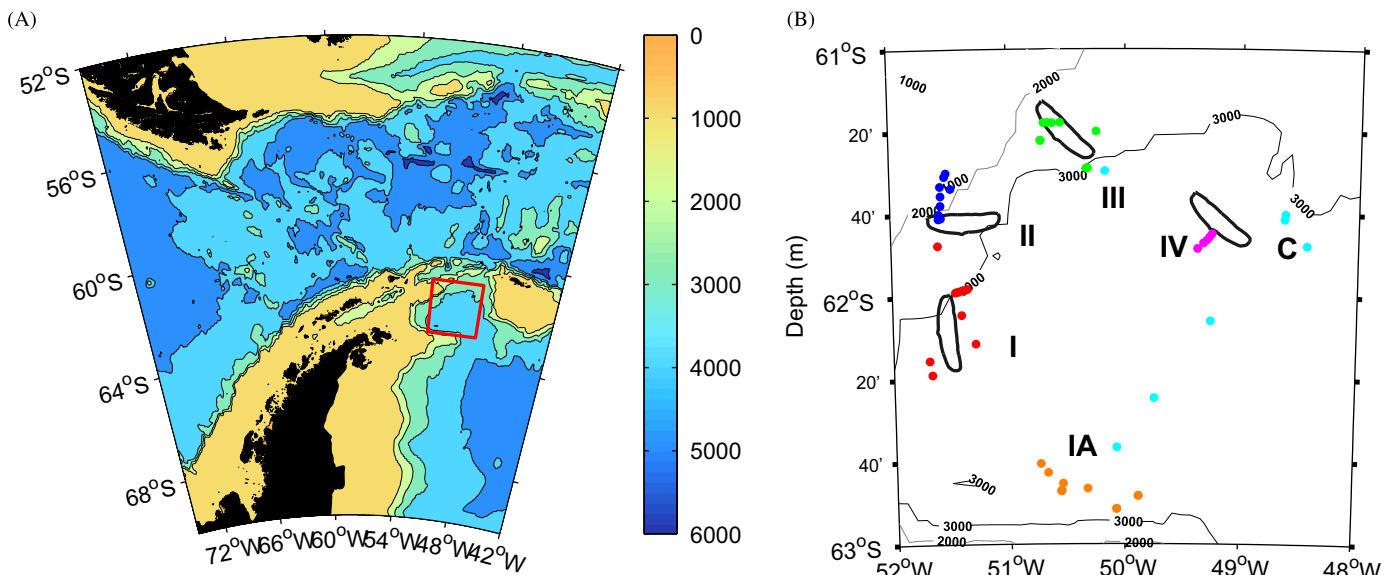
(A)

(B)

Fig. 1. (A) Powell Basin is in the northwest Weddell Sea, just east of Drake Passage and the Antarctic Peninsula, south of the Scotia Sea. (B) C-18a travelled clockwise around the Powell Basin; the estimated positions on March 11 (I), March 22 (II), March 31 (III), and April 10 (IV) are indicated. CTD casts were collected near C-18a on March 10–17 (red), March 18–22 (blue), March 29-April 2 (green), and April 10–11 (magenta). Sampling occurred in Iceberg Alley (IA, orange) April 4–9. Outside of IA, casts that were more than 50 km from C-18a at the time of survey are grouped together (cyan) and include casts taken April 3–7 at or en route to a reference station (C) and one cast taken ~74 km from C-18a on March 29 (near III). (For interpretation of the references to color in this figure legend, the reader is referred to the web version of this article.)

measurements of Fe and other nutrients are reported elsewhere in this issue (Lin et al., 2011; Vernet et al., 2011). Sampling centered around C-18a followed the same general trajectory as the iceberg (Fig. 1B), resulting in CTD casts spread across the basin, divided here into four regions: I. March 10–17 (red), II. March 18–22 (blue), III. March 29–April 2 (green) and IV. April 10–11 (magenta). Of the 65 CTD casts performed during the cruise, 56 were deeper than 250 m, with most of these profiles going deeper than 500 m. Of the 56 casts deeper than 250 m, 37 occurred within 20 km of C-18a. Of those 37 casts, 23 were between 0.4 and 2 km from the iceberg and 14 were between 2 and 20 km from C-18a. In a region commonly referred to as "Iceberg Alley" (IA, orange) (Ballantyne, 2002; Schodlok et al., 2006), characterized by a high concentration of small icebergs 15 m to 2 km in length, sampling occurred April 4–9 and included 12 CTD casts deeper than 250 m. An additional seven CTD profiles collected outside of IA and farther than 50 km from C-18a at the time of survey occurred March 29 and April 3–7; these casts are grouped together (cyan).

4. Water masses of Powell Basin

Three main water masses—Warm (or Weddell) Deep Water (WDW), Winter Water (WW), and Antarctic Surface Water (AASW)—comprise the upper 500 m of the water column in Powell Basin (Fig. 2). Around 500 m, water properties are characteristic of WDW, with a temperature of 0.5 °C and salinity of 34.6 psu (Solomon et al., 2000). This water mass, a form of Circumpolar Deep Water that is cooled in the Weddell Gyre (Orsi et al., 1993; Rutgers van der Loeff, 1994), varies little across the basin. In the permanent thermocline above the WDW, both temperature and salinity increase with increasing depth with a slope of around 6 °C psu^{-1}. A temperature minimum, also known as the WW, is found in the remnant of the winter mixed layer. Temperature in the WW shows regional variability, with a general decrease to the south, reaching a minimum around −1.7 °C (region IA), compared to −1.3 °C in the north (region III), but all temperature minima occupy a relatively narrow salinity range around 34.4 psu. In the
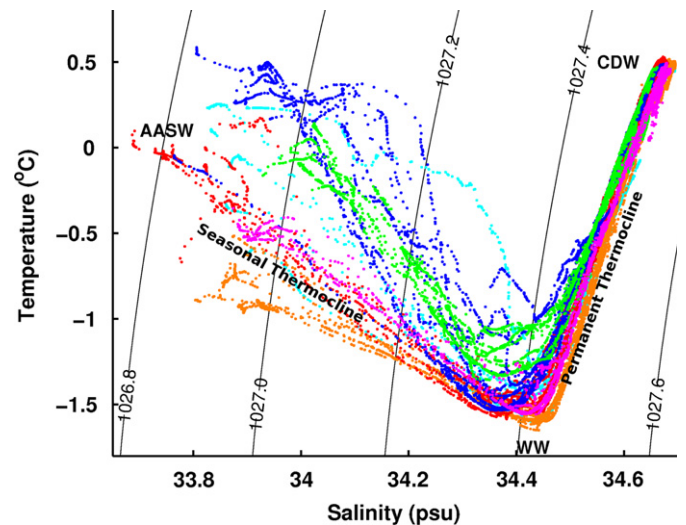

Fig. 2. T–S curves for 56 CTD profiles are grouped by location and time and color-coded as in Fig. 1. CTD casts were collected near C-18a on March 10–17 (red), March 18–22 (blue), March 29–April 2 (green), April 10–11 (magenta), in Iceberg Alley (orange), and far from ice (cyan). A seasonal thermocline lies between the AASW and WW. A permanent thermocline separates WW from WDW. (For interpretation of the references to color in this figure legend, the reader is referred to the web version of this article.)

seasonal thermocline, above the WW layer, temperature increases while salinity decreases with a slope ranging from −1.25 °C psu^{-1} in IA to −4 °C psu^{-1} in regions II and III. Surface water properties range from −1 °C in IA to 0.5 °C near regions II and III with surface salinities near ~33.8–33.9 psu.

The three water masses (WDW, WW, and AASW) form end members to a typical CTD profile in Powell Basin, with the seasonal and permanent thermoclines describing a "V" in T–S space. Deviations from a V-shape occurred in casts taken near the sill separating Powell Basin from the Scotia Sea (Fig. 2, blue), where

large intrusions characteristic of interleaving water masses occur in the surface layer above the temperature minimum, suggesting that bathymetry or advection of water from the Scotia Sea may influence general water properties.

5. Results and discussion

A series of five casts taken over 6 h on a transect from 0.85 to 8.96 km west of C-18a shows a clear impact of ice melt on the subsurface water column (Fig. 3). Over the 8 km of the transect, the WW layer, marked in red in the left-most, closest cast (Fig. 3), decreases in thickness from 150 to 50 m. The average salinity at 50–300 m depth increases with distance from C-18a. Cooler, fresher water near the iceberg suggests the presence of meltwater. To examine the source of this meltwater, we first examine $T–S$ anomalies consistent with meltwater that is turbulently mixed at depth and upwelled. We then characterize the thermohaline steps that indicate melting along a vertical ice face into a salinity gradient. Finally, we make an approximate calculation of the amount of meltwater attributable to each process.

5.1. A meltwater estimate from turbulent processes

Although a thick, well-mixed layer in the profile nearest C-18a in Fig. 3 (WW marked in red) is cooler and fresher than water at the same depth in the other casts from the transect, when $T–S$ properties are compared along isopycnals, this cast appears anomalously warm and salty (Fig. 4A). We use the $T–S$ curve from this cast to illustrate our method for estimating the amount and the concentration of meltwater in the vertical profiles due to turbulent basal melting (Fig. 4B).

To identify water within the warm, salty anomaly, two local temperature minima (points **a** and **b** in Fig. 4B) are selected to define the line L_2, where L_2 is a linear approximation to the "unperturbed" $T–S$ relation. Points on the observed $T–S$ curve between **a** and **b** are therefore anomalously warm and salty relative to L_2. Points **a** and **b** also define the vertical extent of the warm intrusion; for the cast shown in Fig. 4B, they correspond to the depth range from (**a**) 84 m to (**b**) 97 m.

For mixing to produce water with the $T–S$ properties of this anomaly requires the upward displacement of warm, salty water from below the WW layer. We expect melting at the base of the iceberg to produce fresh, cold water. If this water mixes turbulently with ambient water, the resulting water will have a temperature that falls along a line of slope $(\partial T/\partial S)_{melt}$, defined by Eq. (1). The right-hand side of Eq. (1) is calculated using the temperature and salinity data for each cast. The mean value of $(\partial T/\partial S)_{melt}$ over the upper 300 m of a profile is then used as the slope of the meltwater mixing line, L_1. For the example shown in Fig. 4B, the mean value of $(\partial T/\partial S)_{melt}$ over this depth range is 2.36 ± 0.05 °C psu^{-1}, where the uncertainty is computed as twice the standard deviation of $(\partial T/\partial S)_{melt}$ over the upper 300 m. In Eq. (1), changes in ΔT and S are small relative to L and the mean value of S, so variations in $(\partial T/\partial S)_{melt}$ are small.

The meltwater mixing line, L_1, serves as an upper bound to the anomalous $T–S$ region found between **a** and **b**. A line with slope $(\partial T/\partial S)_{melt}$ can pass through each point in the anomaly between **a** and **b**. Here we choose the line L_1 that is tangent to the $T–S$ anomalies such that the intercept at $S=0$ occurs at the maximum possible value for T. For the intrusion between **a** and **b** in the cast shown in Fig. 4B, the meltwater line L_1 is defined by

$$T(S) = (2.36 \pm 0.05) \times S - 82.4 \pm 0.2, \qquad (3)$$

where T has units of °C and S is the salinity. The uncertainty in the intercept is twice the standard deviation of all possible T-intercept values for lines passing through the $T–S$ points between **a** and **b**.

The minimum temperature and salinity required for basal melting to produce the observed anomaly occurs where L_1 intersects the ambient $T–S$ curve at point **c** (Fig. 4B). Point **c** defines the location in the permanent thermocline where the absolute value of the temperature difference between the ambient $T–S$ curve and the $T–S$ values defined by L_1 is a minimum. Uncertainties in the temperature and salinity at point **c** (T_c and S_c) are estimated by propagating uncertainties in the equation for L_1 to the intersection point **c**. The depth of point **c** then defines the minimum source depth, Z_{source}, of the upwelled meltwater. The uncertainty in Z_{source} is estimated as the uncertainty in T_c divided by the mean $\partial T/\partial z$ calculated over a 20 m depth range centered at Z_{source}. In the case shown in Fig. 4B, $T_c = -1.02 \pm 0.18$ °C, $S_c = 34.50 \pm 0.04$ psu and $Z_{source} = 253 \pm 20$ m.
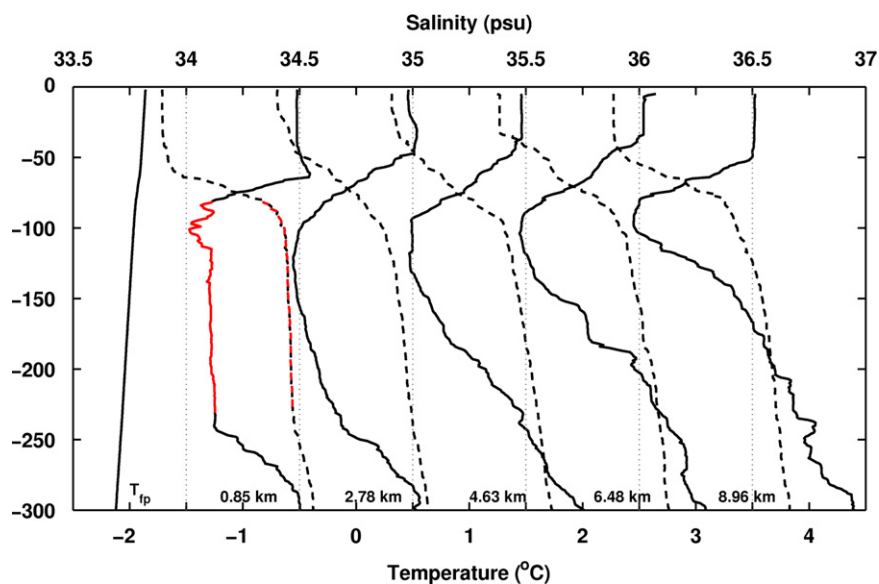

Fig. 3. The freezing temperature of seawater (T_{fp}, solid line at left), temperature (solid) and salinity (dash-dot) profiles with 1 °C and 0.5 psu offsets (left to right) 0.85, 2.78, 4.63, 6.48, and 8.96 km west of C-18a collected over a 6-hour period April 10–11 (Region IV, magenta in Fig. 1B). The Winter Water layer in the cast 0.85 km from C-18a is highlighted in red. (For interpretation of the references to color in this figure legend, the reader is referred to the web version of this article.)
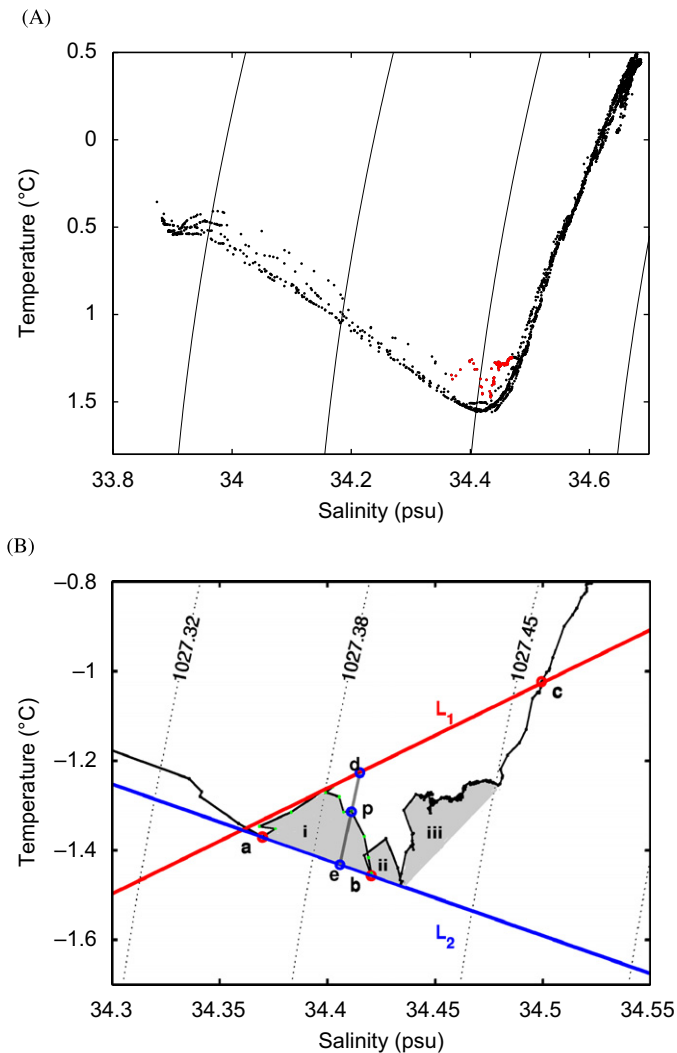
(A)

(B)

Fig. 4. (A) T–S diagrams of casts taken 10–11 April (IV, magenta in Fig. 1). The cast 0.85 km from C-18a (see Fig. 3) shows warm and salty anomalies in the temperature-minimum layer (red). (B) Expanded view of a warm, salty anomaly (**i**) bounded by points **a** and **b**, illustrating the meltwater estimation procedure outlined in the text. A point **p** in the anomaly is modeled as an along-isopycnal mixture of water at **d** from the meltwater mixing line, L_1, and water at **e** from a linear approximation to the ambient T–S relation, L_2. The temperature and salinity required for basal melting to produce the anomaly (**i**) occurs where L_1 intersects the ambient T–S curve at **c**. Two additional anomalies (**ii** and **iii**) are evident in this cast. (For interpretation of the references to color in this figure legend, the reader is referred to the web version of this article.)

To estimate the amount of meltwater contained in the anomalous T–S region between **a** and **b**, we consider water properties along L_1 as a dilution of the ambient water at **c**. Thus, the concentration of meltwater, M, is determined by

$$M(S) = \frac{S_c}{S} - 1,$$ (4)

where S is the salinity along L_1. In Fig. 4B, for the small range of S (34.36–34.43 psu) for which intrusions occur, M ranges from 0.20–0.41%. The uncertainty in S_c of ± 0.04 psu leads to an uncertainty in the meltwater concentration at each point of $\pm 0.11\%$. Since L_2 is an approximation to the background T–S relation, we take the concentration of meltwater along this line to be 0.

Points that fall between lines L_1 and L_2 can be described as a linear combination of water from L_1 and water from L_2. Assuming that the water from L_1 and L_2 mixes along isopycnals, and that water at T–S point **p** is a combination of water with properties **d**

and **e** (Fig. 4B), we solve

$$T_p = \alpha T_d + (1-\alpha)T_e,$$ (5)

for α, the relative contribution of water from L_1,

$$\alpha = \frac{T_p - T_e}{T_d - T_e},$$ (6)

where T_p is the temperature at **p**, T_d is the temperature at **d** and T_e is the temperature at **e** (Fig. 4B). T_d and T_e are the temperatures at which the isopycnal through **p** (gray line, Fig. 4B) intersects L_1 and L_2, respectively. Uncertainty in L_1, described above, leads to uncertainty in T_d. Uncertainty in T_e is due to uncertainties in the slope and intercept of L_2, which result from measurement errors in temperature (± 0.001 °C) and salinity (± 0.01 psu). Eq. (6) is non-linear (particularly for small values of $T_d - T_e$); uncertainties in α are, therefore, determined using a Monte Carlo approach to perturb T_d and T_e by their estimated uncertainty. At the point **p** in the cast shown in Fig. 4B, α is 0.57 ± 0.20. The meltwater fraction at **p** is equal to $0.15 \pm 0.09\%$, which is a product of the meltwater fraction at point **d** ($M_d = 0.26 \pm 0.11\%$) and the relative contribution $\alpha(0.57 \pm 0.20)$ of water with properties at **d**.

Integrating α over the depth range of the T–S anomaly gives the amount of upwelled water in an intrusion. The water column corresponding to the T–S region between **a** and **b** in Fig. 4B contains 7.2 ± 2.6 m³ of water per m² horizontal area that has upwelled from 253 ± 20 m to a new depth of 84–97 m, a vertical displacement of more than 150 m. Integrating αM over intrusion **i** (Fig. 4B) yields an integrated meltwater content of $2.2 \pm 1.2 \times 10^{-2}$ m³ per m² area. Two more anomalies in the cast depicted in Fig. 4b (**ii** and **iii**) contribute an additional $9.0 \pm 5.0 \times 10^{-2}$ m³ per m² area of freshwater to the WW layer with 91.6 ± 29.0 m³ of water upwelled from 246 ± 2 m into the depth range 97–240 m. This estimate of the amount of water upwelled due to meltwater injection at the base of the iceberg is sufficient to explain the 100 m increase in WW layer thickness in this cast relative to casts farther away (Fig. 3).

Meltwater intrusions similar to that shown in Fig. 4B were identified in 11 of the 23 casts closer than 2 km to C-18a, in 5 of the 12 casts in Iceberg Alley, and in 1 cast 17 km from C-18a (Table 1). These T–S anomalies are smaller than the large excursions hypothesized as due to water mass interleaving found in casts near the sill to the northwest of Powell Basin (see for example blue casts in Fig. 2). The slopes of the T–S anomalies due to meltwater intrusions are generally close to the ~ 2.4 °C psu^{-1} typical of meltwater mixing lines. Their appearance in casts close to icebergs and the absence in casts in the same region but farther from icebergs suggest a local source. Most meltwater intrusions were found in region I (Fig. 1B, red). The meltwater intrusion identified in the cast 17 km from C-18a may be associated with a smaller iceberg observed in the vicinity at the time of the CTD cast.

A summary of the depth range of meltwater intrusions observed in these casts, the associated volume of meltwater and upwelled water, and the estimated source depth of meltwater is presented in Table 1. Warm, salty anomalies in T–S diagrams occurred primarily within the WW layer and at the base of the seasonal thermocline. For casts closer than 2 km to C-18a, the anomalies occurred over a range of depths from 67 to 240 m, although a typical vertical extent of meltwater intrusions was ~ 27 m. Three casts that were less than 1 km from C-18a showed multiple meltwater intrusions within one profile. Estimates of Z_{source} from casts within 2 km from C-18a ranged from 163 to 305 m, with a median depth of ~ 233 m, consistent with the iceberg keel depth of at least 190 m from direct observations (Helly et al., 2011). In Iceberg Alley, which was populated by icebergs much smaller than C-18a, intrusions occurred in a narrower depth range of about 76–158 m (Table 1) and were typically ~ 25 m thick. Estimates of Z_{source} for the cast 17 km from C-18a and casts in IA were generally much shallower

Table 1
Properties of meltwater intrusions in 11 casts closer than 2 km to C-18a, 1 cast 17 km from C-18a, and 5 casts in Iceberg Alley. The intrusion depth range of the warm, salty T–S anomalies are indicated. Source depth of meltwater mixtures and the volumes (per m² area) of meltwater and upwelled water in the intrusion are estimated as described for Fig. 4B in the text. Error bars are computed as described in the text.

Cast #	Distance to C-18a (km)	Region	Intrusion depth (m)	Z_{source} (m)	Vol. meltwater (10^{-2} m³)	Upwelled vol. (m³)
19	0.4	II	130–154	270 ± 18	6.0 ± 2.5	11.2 ± 4.7
25	0.4	III	67–88	241 ± 7	4.8 ± 1.3	8.8 ± 4.7
2	0.6	I	83–135	234 ± 24	10.2 ± 4.5	19.2 ± 10.4
			135–175	205 ± 7	3.3 ± 1.7	19.2 ± 7.3
9	0.6	I	72–77	163 ± 14	1.4 ± 0.5	2.7 ± 1.0
1	0.7	I	97–120	244 ± 6	2.6 ± 0.9	5.7 ± 5.5
			120–150	231 ± 4	7.6 ± 2.0	21.6 ± 5.8
			150–189	220 ± 7	2.7 ± 1.1	11.5 ± 6.5
10	0.7	I	83–107	228 ± 20	2.7 ± 0.9	6.2 ± 4.2
65	0.85	IV	84–97	253 ± 20	2.2 ± 1.2	7.2 ± 2.6
			97–101	241 ± 11	0.3 ± 0.2	2.0 ± 0.9
			101–240	246 ± 3	8.7 ± 4.8	89.6 ± 28.1
5	1.2	I	97–165	180 ± 7	5.3 ± 2.9	24.4 ± 11.5
30	1.7	III	202–208	305 ± 32	0.9 ± 0.5	1.9 ± 1.3
6	1.8	I	97–134	202 ± 7	4.6 ± 2.1	17.4 ± 6.8
16	1.8	II	136–182	213 ± 8	2.9 ± 1.2	12.8 ± 8.5
3	17.2	I	81–90	132 ± 5	0.6 ± 0.3	3.7 ± 2.2
41	–	IA	76–98	145 ± 7	1.3 ± 0.7	6.9 ± 4.2
50	–	IA	92–118	136 ± 3	1.1 ± 0.5	10.2 ± 4.5
51	–	IA	82–106	124 ± 10	1.6 ± 0.7	9.8 ± 4.6
52	–	IA	121–158	164 ± 2	0.7 ± 0.3	8.7 ± 7.1
55	–	IA	96–117	125 ± 2	0.8 ± 0.3	8.7 ± 3.6

than those near C-18a, ranging from 124 to 164 m, at a median depth of $\sim$ 138 m (Table 1). Smaller icebergs in IA are likely to have shallower keels than C-18a, consistent with these estimates of meltwater source depth.

The apparent source depth of meltwater intrusions near C-18a showed dependence on the position of a cast relative to fixed points on the iceberg. Although C-18a rotated and translated over the course of the study, when CTD cast locations are considered relative to the iceberg's major axis, a pattern emerges. To describe these variations, we use a north–south orientation of the iceberg's major axis (as depicted near region I, Fig. 1B) to describe the positions of CTD casts with meltwater intrusions (Table 1). Beginning with casts near the northwestern tip of C-18a and moving counter-clockwise, estimates of Z_{source} ranged from 270 to 305 m, decreased to 228–253 m at the midpoint of the iceberg's long edge and had a minimum of 163 m near the southern tip. Continuing counter-clockwise from the southern tip, Z_{source} increased to 180–213 m at the midpoint of the iceberg's eastern edge and to 240 m in casts taken near the northeast corner of C-18a. These variations in source depth may indicate that the northwest side of C-18a (in the north–south orientation depicted near region I) was thicker than the southeast side. These differences in thickness could have originated before C-18 initially calved, as a result of melting at the seaward edge of the iceshelf. Enhanced melting along the leading edge of the iceberg, ahead of the iceberg's direction of motion, could also lead to preferential thinning along that side of the iceberg.

Variations in Z_{source} could also result from variations in the depth of the permanent thermocline. We have assumed that each cast is representative of the conditions where melting occurs, but as Fig. 3 shows, the permanent thermocline may shoal with distance from C-18a. Because water at a given source temperature and salinity is likely to be shallower in a cast farther from C-18a than in a closer cast, shallower estimates of Z_{source} may simply reflect differences in thermocline depth with distance from the iceberg. Thermocline depth may also vary with position around the iceberg, reflecting varying degrees of impact by the iceberg on water ahead or behind the direction of motion of the iceberg. Water ahead of the iceberg's leading edge may be less influenced by meltwater (although it contains upwelled intrusions), have a shallower permanent thermocline, and as a result produce shallower estimates of Z_{source}.

The volume of meltwater in any one profile due to these upwelled intrusions spanned an order of magnitude from 0.6 to 13.5×10^{-2} m³ per m² (Table 1). The volume of upwelled water was also highly variable, and was 2–3 orders of magnitude higher than the volume of meltwater, reflecting the low concentrations of meltwater within an intrusion. In a typical meltwater intrusion near C-18a, O(10 m³) water from the permanent thermocline is vertically displaced by O(100 m). Larger volumes of meltwater and upwelled water occurred in those casts less than 2 km from C-18a, where the median meltwater content in an intrusion was $\sim 2.8 \times 10^{-2}$ m³ per m² horizontal area and the median volume of upwelled water was $\sim$ 11.3 m³, displaced vertically by $\sim$ 93 m. Farther from C-18a and in IA, the volume of meltwater in a typical intrusion was $\sim 1 \times 10^{-2}$ m³ per m², with an associated $\sim$ 8.7 m³ per m² of water in the permanent pycnocline displaced $\sim$ 30 m upwards.

An intermittent physical mechanism for these meltwater intrusions could explain their localization and the variability of their meltwater content. If meltwater at the base of an iceberg is well-mixed, it would produce a less dense mixture of meltwater whose upward motion is constrained by the keel of the iceberg. This positively buoyant water would occasionally "spill" upwards from the edge of the iceberg and rise to a depth at which it is neutrally buoyant. Mixing with water as it rises or at its new density level would move the T–S properties away from the meltwater mixing line, resulting in T–S anomalies whose core has a slope near 2.4 °C psu^{-1} and whose sides relax towards the ambient T–S curve. Several discrete upwelling events like this could explain the casts that exhibited multiple intrusions; such an intermittent mechanism would also explain why many casts close to icebergs did not display these intrusions and why such a large range of upwelled volumes was observed.

5.2. A meltwater estimate from double-diffusive processes

Melting along the vertical sides of an iceberg is a second source of freshwater that can ultimately be entrained into horizontally

stratified layers. Unlike the intrusions associated with upwelled basal meltwater, these layers are not evident in T–S diagrams, but are instead visible as steps in profiles of temperature, salinity, and density. As an example, steps are evident in profiles of potential density in two casts taken an hour apart at distances 0.4 km (Fig. 5A, left) and 1.3 km (Fig. 5A, right) from C-18a on 22 March 2009 (at 51.59°W, 61.68°S and 51.59°W, 61.67°S, respectively, blue in Fig. 1B). These thermohaline steps possess several of the qualities found in laboratory studies (HT80). One expected feature of layers formed by sidewall melting in a salinity gradient is an upward tilt away from the cooling source (HT80; Malki-Epshtein et al., 2004).
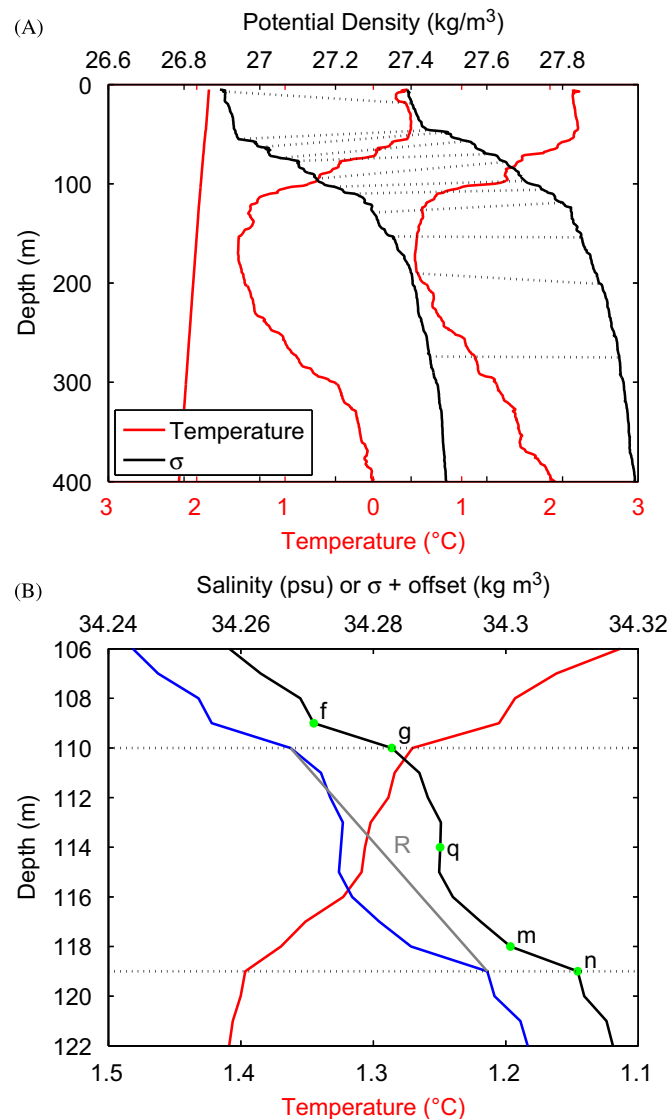

Fig. 5. (A) The freezing temperature (red line, left) and profiles of temperature (red) and potential density (black) in two casts taken 1 h apart 0.4 km (left) and 1.4 km (right) south of C-18a, March 22 (blue in Fig. 1B). The profile on the right is offset 2 °C and 0.2 kg m^{-3}. Isopycnals (dotted line) slant upwards away from the ice in 50–100 m depth range, so that steps in temperature and potential density in the cast at 0.4 km are evident at the same potential densities in the cast at 1.4 km, shifted vertically by ~ 12 m. (B) Expanded view of a step in temperature (red), salinity (blue) and potential density (offset by −992.99 kg m^{-3}) (black) in the cast 0.4 km from C-18a (left profile in (A)), illustrating the step-finding procedure outlined in the text. The interfaces at **f** and **m** have lower bounds at **g** and **n**, respectively, at depths indicated by the dotted lines. A minimum in $\partial\sigma/\partial z$ is found at **q**. R is drawn tangent to the salinity/depth profile at the depths of **g** and **n**. The area between R and the salinity-depth profile (blue line) defines the salinity deficit. (For interpretation of the references to color in this figure legend, the reader is referred to the web version of this article.)

In both casts in Fig. 5A, steps appear at the same potential densities, but are displaced upwards by ~ 12 m in the more distant cast (Fig. 5A, right), suggesting that layers are coherent over a distance of at least 0.9 km. The two casts shown in Fig. 5 confirm that isopycnals slope upwards away from the ice face, as suggested by HT80. Another expected feature of the circulation cells is freshening with depth within a layer due to entrainment of meltwater into the outward-flowing circulation (HT80; Malki-Epshtein et al., 2004). Here we find negative values of the salinity gradient with depth, $\partial S/\partial z$, occur over short depth intervals within a generally positive salinity gradient (e.g. at 113–115 m depth in Fig. 5B, Table 2), showing evidence of local freshening.

The circulation cells set up by double-diffusion at an ice face consist of layers of uniform density, bounded above and below by interfaces, where strong gradients occur. To identify possible interfaces in the 56 CTD casts deeper than 250 m, we determined local maxima in the vertical gradient of potential density, $\partial\sigma/\partial z$, (points **f** and **m** in Fig. 5B). We considered only points where $\partial\sigma/\partial z$ exceeded a threshold of 4×10^{-3} kg m^{-3} dbar^{-1}, approximately twice the mean of $\partial\sigma/\partial z$ over the upper 300 m of casts close to C-18a. Furthermore, a layer was identified only if the minimum value of $\partial\sigma/\partial z$ (**q** in Fig. 5B) between two adjacent interfaces was at least 4×10^{-3} kg m^{-3} dbar^{-1} smaller than $\partial\sigma/\partial z$ at both interfaces (**f** and **m** in Fig. 5B). Use of a smaller threshold increased the number of layers identified as steps and resulted in smaller average step sizes. A larger threshold had the opposite effect, finding fewer, larger steps. However, varying the threshold by 1×10^{-3} kg m^{-3} dbar^{-1}, resulted in no significant change in estimates of the salinity deficit, nor in the resulting freshwater estimate associated with the steps. In some instances where potential density gradients were small, such as below ~ 150 m, the use of the 4×10^{-3} kg m^{-3} dbar^{-1} threshold caused two or more step-like features separated by a weak gradient to be counted as one layer. Prior studies (e.g. Jacobs et al., 1981; Ohshima et al., 1994) that observed small steps embedded in larger steps identified the main layers with the stronger gradients as steps; where such steps occurred, we have done likewise.

The thickness of a layer bounded by the two interfaces (**f** and **m** in Fig. 5B) is measured from the bottom of the upper interface (**g**) to the bottom of the lower interface (**n**). The bottom (**g** or **n**) of an interface (**f** or **m**) is identified as the shallowest local minimum in $\partial^2\sigma/\partial z^2$, where $\partial\sigma/\partial z$ is less than the mean potential density gradient between the two interfaces (**f** or **m**). Given the 1 m resolution of the CTD data, the minimum observable layer thickness with this method is 2 m.

In the upper 300 m of the 56 CTD casts considered, 850 layers were identified using this methodology. In Table 2, we compare step properties for casts at different distances from the iceberg: closer than 2 km from C-18a; in a range 2–20 km from C-18a; in IA (orange, Fig. 1B); and in casts far from ice (cyan in Fig. 1B). Typically, ~ 15 layers were found in each cast, irrespective of distance from the iceberg. Layers were characterized by average changes in temperature of approximately −0.05 °C, changes in potential density of approximately 0.023 kg m^{-3}, and salinity changes of approximately 0.027 psu on average, except in IA which had larger salinity and density changes and smaller temperature changes (Table 2). Layers most commonly appeared above the WW with a mean depth of ~ 84 m, except in IA where the mean depth of the isopycnal layers was ~ 57 m (Table 2). The mean layer thickness agreed within two standard errors, ranging from 7.3 ± 7.9 m in the casts far from the iceberg (C in Fig. 1B) to 9.1 ± 6.3 m for those casts less than 2 km from C-18a. The average minimum salinity gradient, $\partial S/\partial z$, was weakly negative (~ −2.4 ± 2.0 × 10^{-3} psu m^{-1}) for those casts closer than 2 km to C-18a. Farther from C-18a and in IA, the average minimum $\partial S/\partial z$ in a layer was not significantly different from zero. This suggests that freshening with depth

Table 2

Mean properties ($\pm$ twice the standard error) of themohaline steps in profiles of potential density from CTD casts less than 2 km from C-18a, between 2 and 20 km from C-18a, in Iceberg Alley, and other casts far from ice. The reported depth of a layer is the depth of its midpoint. Layer thickness is the distance between the bases of the interfaces that define the layer. $\Delta\sigma, \Delta T$ and ΔS are the change in potential density, temperature, and salinity across a layer. The minimum salinity gradient, $\partial S/\partial z$, observed within each layer is averaged over the casts in each group. The salinity deficit within a layer is computed as outlined in the text. The freshwater excess is the amount of freshwater required to account for the integrated salinity deficit in each cast.

Profile group	< 2 km	2–20 km	Iceberg Alley	Other
Number of casts	23	14	12	7
# of layers per cast	16.7 ± 1.7	14.9 ± 2.1	12.4 ± 1.2	15.6 ± 1.6
Depth of layers (m)	89.5 ± 20.1	78.9 ± 15.7	57.2 ± 12.4	82.9 ± 14.1
Layer thickness (m)	9.1 ± 6.3	7.3 ± 5.3	7.4 ± 6.3	7.3 ± 7.9
$\Delta\sigma$ (10^{-2} kg m^{-3})	2.2 ± 0.9	2.3 ± 0.8	3.1 ± 1.0	2.5 ± 0.9
ΔT (10^{-2} °C)	5.4 ± 4.7	-5.6 ± 4.9	-2.1 ± 6.0	-3.5 ± 8.8
ΔS (10^{-2} psu)	2.6 ± 1.0	2.7 ± 1.0	3.9 ± 1.2	3.0 ± 1.2
Minimum of $\partial S/\partial z$ (10^{-3} psu m^{-1})	-2.4 ± 2.0	-2.0 ± 2.6	0.6 ± 2.0	-1.9 ± 2.6
Salinity deficit/step (10^{-2} g cm^{-2})	4.2 ± 3.5	3.3 ± 2.6	4.0 ± 5.0	2.2 ± 1.3
Freshwater excess/cast (10^{-2} m^3 per m^2)	18.5 ± 4.7	12.9 ± 4.1	13.5 ± 4.7	9.1 ± 1.5

within a layer, a feature of circulation cells suggested by HT80, is more evident in casts closer to C-18a.

To test the predictions of layer thickness made by HT80, we computed h from Eq. (2) using the temperature and salinity from each cast and the freezing temperature calculated using the salinity–pressure profile. Potential density was used in place of density in Eq. (2), and for each cast the vertical gradient in potential density, $\partial\sigma/\partial z$, was averaged with a 50-point running mean.

While the laboratory experiments of HT80 were performed in a uniform density gradient and at constant temperature, the environment of the Weddell Sea has neither of these features. Variations in salinity, temperature, and $\partial\sigma/\partial z$ with depth (e.g. Fig. 5A) lead to a vertically varying predicted layer thickness, h (Fig. 6A). Predicted layer thickness reaches a minimum of about 2.5 m in the temperature-minimum layer, where water as cool as -1.5 °C is already close to the depressed freezing point (Fig. 5A).

Observed and predicted layer thicknesses for each step identified in the potential density profiles were binned by depth and averaged (Fig. 6B). Agreement between observed and predicted layer thickness is best from 40 to 100 m depth (Fig. 6B). In the surface mixed layer, air-sea heat flux and wind forcing mix out any stratified step structure, resulting in very few layers being identified in the upper 50 m. The resulting low stratifications in the surface mixed layer lead to a breakdown in Eq. (2). This suggests that, in the surface layer, the dominant direction of meltwater motion is upwards, and also that double-diffusive melting into stratified layers may not be a relevant mixing process in this part of the water column.

Thicker layers observed below the temperature minimum (130–180 m in Fig. 5A) could be due to merging of two or more smaller layers with distance from the iceberg. Greater buoyancy of meltwater at depth results in meltwater that rises more quickly, which could lead to thicker layers at greater depth. Below the temperature minimum, water that is cool and fresh overlies warmer, saltier water and diffusive convection can occur, rather than salt-fingering, which may also enhance layer thickness.

Following Jacobs et al. (1981), we estimate the amount of meltwater present in the thermohaline steps by assuming that a salt deficit can be defined by the area between the salinity-depth profile of a typical thermohaline step and a line drawn tangent (**R** in Fig. 5B) between the bases of the two interfaces (**g** and **m**) that define the step (dashed lines in Fig. 5B). Water at the tops of the circulation cells (at **g** and **m**) is ambient water cooled slightly as it is drawn in towards the ice; it has the salinity of the ambient water, making line **R** a linear approximation to the background salinity profile.

Physically, we also assume that the observed steps are formed by the addition of freshwater to the water column and are not due
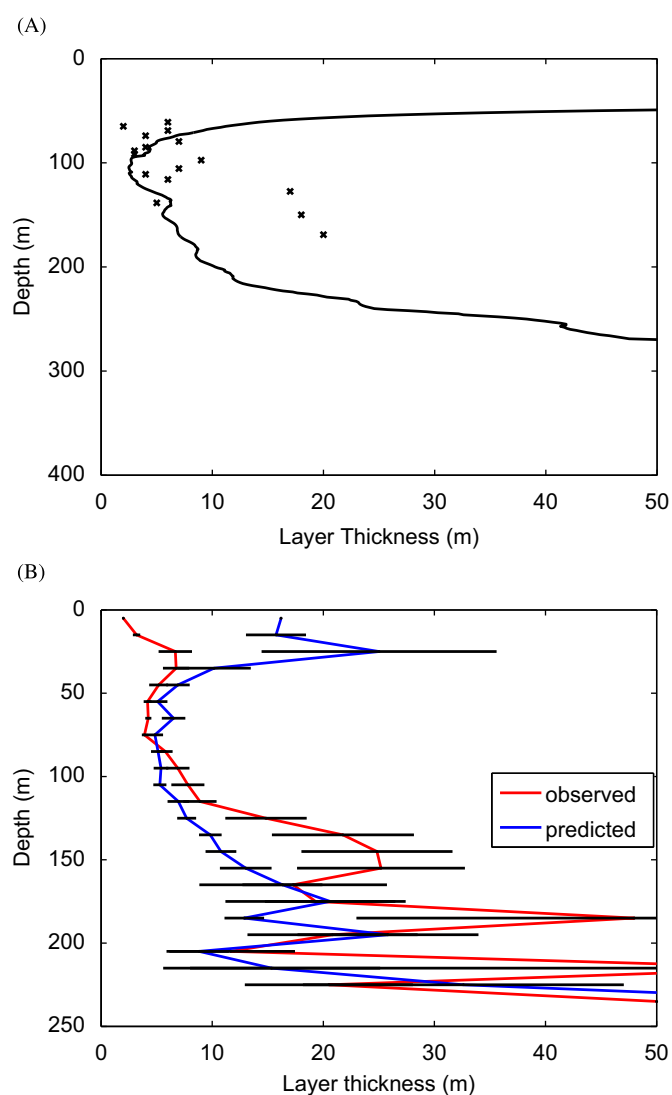
(A)

(B)

Fig. 6. (A) Observed layer thickness (x) and layer thickness predicted from Eq. (2) (solid line), calculated from temperature and salinity data for the profile at 0.4 km in Fig. 5A. Layer thickness is at a minimum in the temperature minimum layer and increases below 200 m. (B) Mean observed (red) and predicted (blue) layer thicknesses binned by depth for all layers identified in potential density profiles. Where layers were observed, predicted layer thickness (red) is calculated as the average value of h in Eq. (2) over the depth range of the layer. Black lines indicate standard error. Layer thickness agrees most closely in the 40–100 m depth range, averaging about 5 m. (For interpretation of the references to color in this figure legend, the reader is referred to the web version of this article.)

to a rearrangement of T and S within the water column. Where the water column is diffusively stable (warm, fresh water over cool, salty water), as it is in the seasonal thermocline above the WW layer, diffusive convection and salt-fingering do not occur, suggesting that sidewall melting could be the predominant cause of the steps. The salinity deficit for the case pictured in Fig. 5B is 0.05 psu m, equivalent to a deficit of about 0.05 g cm^{-2} salt or the addition of 1.5×10^{-2} m^3 freshwater to a 1 m^2 area of the water column.

In casts closer than 2 km to C-18a (Table 2), steps with a mean (± 2 standard errors) salinity deficit of 0.042 ± 0.035 g cm^{-2} imply a freshwater excess of 1.23 ± 1.03 cm per step. The amount of freshwater in layers at other sites agreed within two standard error bars (Table 2), but the average freshwater excess in a typical layer in IA was not significantly different from zero. Integrating the freshwater excess over each cast, we find that the total freshwater contribution in the upper 300 m of a 1 m^2 water column due to sidewall melting is O(0.1–0.2 m^3).

6. Conclusions

At least two modes of meltwater mixing appear to contribute freshwater to the region near C-18a. Warm, salty anomalies appear primarily in CTD casts taken less than 2 km from the iceberg. The amount of meltwater, the proximity to the iceberg, and the close match in T–S space with the slope of the predicted meltwater mixing line are consistent with upwelled mixtures of basal melt and ambient water near the base of the iceberg. Upwelled basal meltwater is highly variable in space, and appears to be localized; intrusions are detectable mostly within about 2 km of the iceberg. Only half of the casts within 2 km of C-18a exhibited these intrusions, suggesting that upwelling of meltwater mixtures may be an intermittent process. Where basal melting occurs, it appears to be responsible for O(0.1^3) of freshwater in a 1 m^2 water column. A small amount of ice is melted, cooling and freshening a much larger volume of water from the permanent thermocline. This water does not rise all the way to the surface, but instead finds a neutrally buoyant level at the base of the seasonal thermocline, where it forms a thick layer of water that, although slightly warmer than the ambient WW at the same density, is cool relative to the AASW and WDW. This supports the idea suggested by Jacobs et al. (1979) that icebergs may play a role in maintaining the WW layer.

The highly variable nature of the upwelling basal meltwater mixtures may contribute to the observed patchiness in micronutrient supply (Lin et al., 2011) and in the phytoplankton (Vernet et al., 2011) and zooplankton (Kaufmann et al., 2011) communities near C-18a. Vertical nutrient transport can stimulate primary production, but the initial effect of a large injection of deeper water (from $\sim$200 m) into the euphotic zone (estimated to be 50–100 m deep, Vernet et al., 2011) is likely to be a dilution of phytoplankton populations. This may be a factor in the delay between passage of an iceberg and increased productivity in its wake (e.g. Schwarz et al., 2009; Helly et al., 2011).

Thermohaline steps consistent with melting from a vertical ice face are ubiquitous in profiles in this region, especially in the depth range 40–100 m. These steps exhibit many of the properties of the meltwater layers observed in the tank experiments of HT80. The average thickness of layers associated with steps in the seasonal thermocline matches that predicted by Eq. (2). Layers appear to be continuous over short distances and tilt upwards with distance from the iceberg. Freshening towards the bottom of the steps is also observed. The amount of freshwater contained in thermohaline steps within a 1 m^2 water column is $\sim$0.1−0.2 m^3, similar to the estimated freshwater ascribed to upwelled basal meltwater mixtures. This value is 2–3 times larger than the 0.06 m^3 per m^2 that Jacobs et al. (1981) observed near the Erebus Glacier Tongue, where conditions were much cooler.

The appearance of these steps in all of the casts we examined, even far from ice, and in a diffusively stable part of the water column suggests that they are stable and that the influence of melting ice is discernible across the Powell Basin. Horizontal spread of meltwater and associated nutrients by double-diffusive circulation cells provides a means by which the seasonal thermocline can be enriched in nutrients from ice melt over a much larger area than turbulent upwelling without diluting microbial and planktonic populations. Near an ice face, where ice is actively melting, advection by shear flow between cells could contribute to the formation of thin, vertically stacked layers in existing patches of plankton, and could act to enhance horizontal dispersal of such patches.

This study confirms that both basal and sidewall melting contribute significant amounts of freshwater to the upper ocean near icebergs. No single mechanism dominates subsurface ice melt. Basal melt induces vertical transport of potentially nutrient-rich water, while sidewall melting has the potential to enrich the thermocline in micronutrients over a large areal extent. The data collected in this study were not sufficient to characterize horizontal variations in subsurface meltwater or the detailed advection of melt water relative to the iceberg. These issues will require further detailed field work.

Acknowledgments

References

Ballantyne, J., 2002. A multidecadal study of the number of Antarctic icebergs using scatterometer data. Brigham Young University online report, ⟨http://www.scp.byu.edu/data/iceberg/IcebergReport.pdf⟩.

Donaldson, P.B., 1978. Melting of Antarctic icebergs. Nature 275, 305–306.

Gade, H.G., 1979. Melting of ice in sea water: a primitive model with application to the Antarctic ice shelf and icebergs. J. Phys. Oceanogr. 9, 189–198.

Gade, H.G., 1993. When ice melts in sea water: a review. Atmos. Oceans 31, 139–165.

Helly, J., Kaufmann, R., Stephenson Jr., G.R., Vernet, M., 2011. Cooling, dilution and mixing of ocean water by free-drifting icebergs in the Weddell Sea. Deep-Sea Res. II 58 (11-12), 1346–1363.

Huppert, H.E., Turner, J.S., 1980. Ice blocks melting into a salinity gradient. J. Fluid Mech. 100, 367–384.

Jacobs, S.S., Gordon, A.L., Amos, A.F., 1979. Effect of glacial ice melting on the Antarctic Surface Water. Nature 277, 469–471.

Jacobs, S.S., Helmer, H.H., Doake, C.S.M., Jenkins, A., Frolich, R.M., 1992. Melting of ice shelves and the mass balance of Antarctica. J. Glaciol. 38, 375–387.

Jacobs, S.S., Huppert, H.E., Holdsworth, G., Drewry, D.J., 1981. Thermohaline steps induced by melting of the Erebus Glacier Tongue. J. Geophys. Res. 86, 6547–6555.

Jenkins, A., 1999. The impact of melting ice on ocean waters. J. Phys. Oceanogr. 29, 2370–2381.

Jongma, J.J., Driesschaert, E., Fichefet, T., Goosse, H., Renssen, H., 2009. The effect of dynamic–thermodynamic icebergs on the Southern Ocean climate in a three-dimensional model. Ocean Modelling 26, 104–113.

Kaufmann, R.S., Robison, B.H., Sherlock, R.E., Reisenbichler, K.R., Osborn, K.J., 2011. Composition and structure of macrozooplankton and micronekton communities in the vicinity of free-drifting Antarctic icebergs. Deep-Sea Res. II 58 (11-12), 1469–1484.

Lin, H., Rauschenberg, S., Hexel, C.R., Shaw, T.J., Twining, B.S., 2011. Free-drifting icebergs as sources of iron to the Weddell Sea. Deep-Sea Res. II 58 (11-12), 1392–1406.

Malki-Epshtein, L., Phillips, O.M., Huppert, H.E., 2004. The growth and structure of double-diffusive cells adjacent to a cooled sidewall in a salt-stratified environment. J. Fluid Mech. 518, 347–362.

Morell, J.M., Corredor, J.E., Merryfield, W.J., 2006. Thermohaline staircases in a Caribbean eddy and mechanisms for staircase formation. Deep-Sea Res. II 53, 128–139.

Neshyba, S., 1977. Upwelling by icebergs. Nature 267, 507–508.

Ohshima, K.I., Kawamura, T., Takizawa, T., Ushio, S., 1994. Step-like structure in temperature and salinity profiles, observed near icebergs trapped by fast ice, Antarctica. J. Oceanogr. 50, 365–372.

Orsi, A.H., Nowlin Jr., W.D., Whitworth III, T., 1993. On the circulation and stratification of the Weddell Gyre. Deep-Sea Res. II 40, 167–203.

Rutgers van der Loeff, M.M., 1994. 228 Ra and 228 Th in the Weddell Sea. American Geophysical Union, Washington, DC, pp. 177–186.

Schmitt, R.W., 1994. Double-diffusion in oceanography. Annu. Rev. Fluid Mech. 26, 255–285.

Schodlok, M.P., Hellmer, H.H., Rohardt, G., Fahrbach, E., 2006. Weddell Sea iceberg drift: five years of observations. J. Geophys. Res. 111, C06018. doi:10. 1029/2004JC002661.

Schwarz, J.N., Schodlok, M.P., 2009. Impact of drifting icebergs on surface phytoplankton biomass in the Southern Ocean: Ocean colour remote sensing and in situ iceberg tracking. Deep Sea Res. I 56, 1727–1741, doi:10.1016/j.dsr.2009. 05.003.

Sherlock, R.E., Reisenbichler, K.R., Bush, S.L., Osborn, K.J., Robison, B.H., 2011. Near-field zooplankton, ice-face biota, and proximal hydrography of free-drifting Antarctic icebergs. Deep-Sea Res. II 58 (11-12), 1457–1468.

Silva, T.M., Bigg, G.R., Nicholls, K.W., 2006. Contribution of giant icebergs to the Southern Ocean freshwater flux. J. Geophys. Res. 111. doi:10.1029/2004JC002843.

Smith, K., Robison, B.H., Helly, J.J., Kaufmann, R.S., Ruhl, H.A., Shaw, T.J., Twining, B.S., Vernet, M., 2007. Free-drifting icebergs: hot spots of chemical and biological enrichment in the Weddell Sea. Science 317, 478–482.

Solomon, H., Ushida, K., Suzuki, T., 2000. Interannual variability of Antarctic hydrographic structure and frontal zones along meridional sections between Syowa station and Southern Africa. J. Oceanogr. 56, 1–16.

Stuart, K.M., Long, D.G., 2011. Tracking large tabular icebergs using the Sea Winds Ku-band microwave scatterometer. Deep-Sea Res. II 58 (11-12), 1285–1300.

Vernet, M., Sines, K., Chakos, D., Cefarelli, A.O., Ekern, L., 2011. Impacts on phytoplankton dynamics by free-drifting icebergs in the NW Weddell Sea. Deep-Sea Res. II 58 (11-12), 1422–1435.